

General variational model reduction applied to incompressible viscous flows

THORSTEN BOGNER†

Theoretical Physics, Universität Bielefeld, 33615 Bielefeld, Germany
bogner@physik.uni-bielefeld.de

(Received 11 October 2007 and in revised form 13 August 2008)

In this paper, a method is introduced that allows calculation of an approximate proper orthogonal decomposition (POD) without the need to perform a simulation of the full dynamical system. Our approach is based on an application of the density matrix renormalization group (DMRG) to nonlinear dynamical systems, but has no explicit restriction on the spatial dimension of the model system. The method is not restricted to fluid dynamics. The applicability is exemplified on the incompressible Navier–Stokes equation in two spatial dimensions. Merging of two equal-signed vortices with periodic boundary conditions is considered for low Reynolds numbers $Re \leq 800$ using a spectral method. We compare the accuracy of a reduced model, obtained by our method, with that of a reduced model obtained by standard POD. To this end, error functionals for the reductions are evaluated. It is observed that the proposed method is able to find a reduced system that yields comparable or even superior accuracy with respect to standard POD method results.

1. Introduction

Dynamical systems arise wherever time-dependent processes have to be described. An important class of problems is given by partial differential equations. These typically arise from physical theories, such as hydrodynamics (see Landau, Lifschitz & Weller 1991), elastic theory (see Leipholz 1974), electrodynamics, etc. Numerical approaches require a discretization of the partial differential equations and can consider only a finite number of degrees of freedom. This leads to a discretization error. Increasing the resolution, i.e. the number of degrees of freedom in the numerical description, typically increases the accuracy. For obtaining reasonable low error bounds this can lead to a high dimensionality of the discretized system. The aim of model reduction is to provide a ‘small’ model system which can describe and reproduce the relevant behaviour of a much larger dynamical system. This is summarized in some detail, e.g. by Antoulas (2005). Orthogonal projection methods are an important class for model reduction schemes. Following this approach, the dynamics of the reduced model is given by a linear projection of the original dynamics to a lower dimensional subspace. If nonlinear systems are also to be considered, an important method for choosing such a subspace is given by the proper orthogonal decomposition (POD), which was introduced by Lumley (1967) (see e.g. Sirovich 1987 for details). To actually calculate a POD, the simulation of the unreduced system is necessary. Recently a method to avoid this constraint for spatial one-dimensional (also nonlinear) systems has been proposed by Bogner (2007). For practical purposes this restriction to

† Email address for correspondence: bogner@physik.uni-bielefeld.de

one-dimensional systems is unfavourable. Here, we extend the approach to a variational method which can be applied to higher dimensional systems. To test the new method we apply it exemplarily to the process of vortex merging in two-dimensional incompressible Navier–Stokes equations.

This paper is organized as follows. First, the description of the dynamical systems is introduced and the model reduction by orthogonal projection is described. Then the POD is reviewed briefly. Also, the variational POD approach is presented. Next, some background to the two-dimensional flow problem at hand and the two-dimensional incompressible Navier–Stokes equations is recalled. The results from the numerical calculations are presented and the error due to the reduction is compared for the different approaches.

2. Description and reduction of the dynamics

We consider a scalar field $q_C(x, t)$, which depends on a spatial variable $x \in \Omega \subset \mathbb{R}^d$ and time t (here we consider $d=2$ for simplicity, but higher values are also possible). The computational domain is Ω . The time evolution of $q_C(x, t)$ is given by a partial differential equation of the form

$$\frac{\partial}{\partial t} q_C(x, t) = \mathcal{G}(q_C(x, t)) q_C(x, t), \quad (2.1)$$

where \mathcal{G} is some (eventually nonlinear) operator that can also contain spatial derivatives. Here we consider autonomous systems, although there is no explicit restriction for the method.

The discretization is obtained by approximating the scalar field $q_C(x, t)$ by an expansion of the form

$$q_C(x, t) \approx q(x, t) := \sum_{i=1}^N q_i(t) \varphi_i(x). \quad (2.2)$$

In this work no base flow is assumed. Expansion (2.2) simply defines the discretization via the Galerkin approach. In (2.2) the $\varphi_i(x)$ constitute a set of orthonormal functions, i.e.

$$\int_{\Omega} \varphi_i(x) \varphi_j(x) dx = \delta_{ij}. \quad (2.3)$$

The dimensionality of the phase space of the discretized system, i.e the number of ansatz functions φ_i , is finite, e.g. $i = 1, \dots, N$. The time dependence of the discretized solution is given by the N -dimensional vector containing the coefficients, i.e. $\mathbf{q} := (q_1, \dots, q_N)$. In this work, the ansatz functions φ_i are Fourier modes, or equivalently, periodic sinc functions (see Gottlieb & Orszag 1977). Both cases are related via a basic change. The resulting dynamics is not affected.

Expressing (2.1) in its weak form and restricting the test functions to the ansatz functions φ_i yields an equation for the time evolution of the discretized system. The resulting ordinary differential equation has the form

$$\frac{d}{dt} q_i(t) = \sum_{j=1}^N \mathbf{G}_{ij}(\mathbf{q}(t)) q_j(t), \quad i = 1, \dots, N, \quad (2.4)$$

where \mathbf{G} is the generator of evolution and depends explicitly on \mathbf{q} for nonlinear problems. Technically, \mathbf{G} is an $N \times N$ matrix that can depend on the discretized field. The particular form of \mathbf{G} results from the dynamical system considered, as well as from the choice of the discretization. For our purposes it is useful to expand $\mathbf{G}(\mathbf{q}(t))$ in powers of the coefficients q_i , $i = 1, \dots, N$. For the set of ordinary differential

equations this expansion yields

$$\frac{d}{dt}q_i(t) = \sum_{j=1}^N \mathbf{L}_{ij}q_j(t) + \sum_{j,k=1}^N \mathbf{Q}_{ijk}q_j(t)q_k(t) + \cdots, \quad i = 1, \dots, N, \quad (2.5)$$

where the contributions \mathbf{L} and \mathbf{Q} represent the linear and the quadratic part of the – typically nonlinear – generator of evolution. For many applications this expansion is truncated. The Navier–Stokes equations have a quadratic nonlinearity. Thus the \mathbf{Q} terms already represent the nonlinearity and there are no higher order terms. The matrix \mathbf{L} is an $N \times N$ matrix, while \mathbf{Q} has three indices running from 1 to N . Likewise, every higher order contribution contains the number of parameters higher by a factor of N than the previous order. Note that these parameters define the dynamics of the system but do not increase the dimensionality of the phase space. There exist some discretizations that cannot be written in the form of (2.5) with a finite number of terms. One of these is the Donor-Cell discretization, described by Gentry, Martin & Daly (1966), as it contains absolute values of the fields.

We start from a discretized system of the type given in (2.4) and (2.5). The dynamic equation (2.1) as well as the ansatz functions φ_i , $i = 1, \dots, N$, and the size N of the discretized system are prescribed. The system given by (2.5) is termed here as the original or full system. We assess the additional error due to model reduction. The discretization error can be controlled typically by choosing the resolution high enough and will not be considered. The reduction is uniquely defined by the projection operator

$$\mathbf{P} = \mathbf{B}\mathbf{B}^\dagger \in \mathbb{R}^{N \times N}, \quad (2.6)$$

where the columns of \mathbf{B} form an orthonormal basis of the reduced phase space and \mathbf{B} is of the form $\mathbf{B} \in \mathbb{R}^{N \times M}$. The dimensionality of the reduced model is $M < N$ (we are interested in the case $M \ll N$) and \mathbf{B}^\dagger is the hermitian conjugate of \mathbf{B} . Different choices of \mathbf{B} can yield the same \mathbf{P} . We will always consider the columns of \mathbf{B} to be mutually orthonormal. To compare the quality of our approach with the standard POD method the value of M is prescribed here. In practice the value of M would be determined by the required accuracy and the available computer resources. The reduced dynamics results from multiplying both sides of (2.5) with \mathbf{P} (since \mathbf{P} is a projector, $\mathbf{P}\mathbf{P} = \mathbf{P}$ holds) and is given by

$$\begin{aligned} \frac{d}{dt} \left(\sum_{j=1}^N \mathbf{P}_{ij}q_j(t) \right)_i &= \left(\sum_{j,k,l=1}^N \mathbf{P}_{ij}\mathbf{L}_{jk}\mathbf{P}_{kl}q_l(t) \right)_i \\ &+ \left(\sum_{j,k,l,m,n=1}^N \mathbf{P}_{ij}(\mathbf{Q}_{jkl}\mathbf{P}_{km}q_m(t)\mathbf{P}_{ln}q_n(t)) \right)_i + \cdots. \end{aligned} \quad (2.7)$$

Note that this equation is still defined in the N -dimensional phase space. However, it determines the solution on the reduced subspace only. By introducing the reduced entities

$$\tilde{q}_i = \sum_{a=1}^N \mathbf{B}_{ia}^\dagger q_a \quad \text{with } \tilde{\mathbf{q}} \in \mathbb{R}^M, \quad (2.8)$$

$$\tilde{\mathbf{L}}_{i,j} = \sum_{a,b=1}^N \mathbf{B}_{ia}^\dagger \mathbf{L}_{a,b} \mathbf{B}_{b,j}, \quad i, j = 1, \dots, M, \quad (2.9)$$

$$\tilde{\mathbf{Q}}_{i,j,k} = \sum_{a,b,c=1}^N \mathbf{B}_{ia}^\dagger \mathbf{Q}_{a,b,c} \mathbf{B}_{b,j} \mathbf{B}_{c,k}, \quad i, j, k = 1, \dots, M, \quad (2.10)$$

we can express the dynamics of the reduced model in an M -dimensional space as

$$\frac{d}{dt} \tilde{q}_i = \sum_{j=1}^M \tilde{\mathbf{L}}_{ij} \tilde{q}_j + \sum_{j,k=1}^M \tilde{\mathbf{Q}}_{ijk} \tilde{q}_j \tilde{q}_k + \dots \quad (2.11)$$

Note that in general the solution of (2.11) yields a $\tilde{q}(t)$ which is different from the one obtained by projecting a full trajectory to the reduced subspace via (2.8). This is due to the fact that the reduction and the time evolution do not necessarily commute for nonlinear systems. For linear systems this is only true if the reduced subspace is invariant under \mathbf{L} .

The error due to the reduction is given by

$$E_i(t) = \left(q_i(t) - \sum_{j=1}^M \mathbf{B}_{ij} \tilde{q}_j(t) \right), \quad i = 1, \dots, N. \quad (2.12)$$

One possible scalar measure for the error is given by the squared Euclidean norm of $\mathbf{E}(t)$,

$$\mathbf{E}(t) = \left\| \left(q_i(t) - \sum_{j=1}^M \mathbf{B}_{ij} \tilde{q}_j(t) \right)_{i=1, \dots, N} \right\|_2^2. \quad (2.13)$$

Due to the normalization condition of the expansion functions (see (2.3)), this error measure is (up to a constant factor) identical with the L^2 -error of the solution function $q(x, t)$ constructed from the coefficients $q_i(t)$ in (2.2).

3. Proper orthogonal decomposition

Given a (discretized) dynamical system (e.g. (2.5)), a set of initial conditions and a time interval of interest, the task is to find an optimal linear projection to reduce (the dimensionality of) the phase space of the system. This is done by the POD systematically. The POD is widely used in model reduction. On this topic an extensive literature exists. Some examples are given by Lorenz (1956), Sirovich (1987), Berkooz, Holmes & Lumley (1998), Rowley, Colonius & Murray (2003) and Noack *et al.* (2003). An explanation of the POD together with the method of snapshots is also given by Sirovich (1987) and Bui-Thanh *et al.* (2003). One of the advantages of this method is the possibility to incorporate information from the nonlinear dynamics to obtain a linear reduction. The basic idea is to generate sample trajectories by simulating the system of interest.

From the dynamic equation (2.5), we can define a time average, if we specify a set of trajectories. The time average of some observable A can be defined by

$$\langle A \rangle_T := \frac{1}{n(t_{max} - t_0)} \sum_{k=1}^n \int_{t_0}^{t_{max}} A(\mathbf{q}^k(t)) dt, \quad (3.1)$$

where n is the number of sample trajectories and $\mathbf{q}^k(t)$ is the state vector for the k th trajectory. The time average is carried out from t_0 to t_{max} and over all sample trajectories \mathbf{q}^k , $k = 1, \dots, n$. The choice of the time interval as well as the choices of the initial conditions for the sample trajectories depend on the process to be studied.

A common optimality condition, also used by Sirovich (1987) and Antoulas (2005), is requiring the average least-square truncation error being minimal. Although this is

not the only sensible choice we will use in this condition, i.e.

$$\epsilon := \langle \mathbf{E}^k(t) \rangle_T = \langle \| \mathbf{q}^k(t) - \mathbf{P}\mathbf{q}^k(t) \|_2^2 \rangle_T \stackrel{!}{=} \text{minimal}. \quad (3.2)$$

Here \mathbf{P} is again the projection operator defined by the reduced orthonormal basis \mathbf{B} (see (2.6)). Instead of minimizing the error ϵ which is the time average of

$$\| \mathbf{q}^k(t) - \mathbf{P}\mathbf{q}^k(t) \|_2^2 = \| \mathbf{q}^k(t) \|_2^2 - 2\langle \mathbf{q}^k(t), \mathbf{P}\mathbf{q}^k(t) \rangle + \| \mathbf{P}\mathbf{q}^k(t) \|_2^2, \quad (3.3)$$

we can maximize the time average of $\langle \mathbf{q}^k(t), \mathbf{P}\mathbf{q}^k(t) \rangle$, i.e. the average projection of $\mathbf{q}^k(t)$ onto itself under \mathbf{P} . The brackets $\langle \cdot, \cdot \rangle$ (without subscript) denote the canonical scalar product (or Euclidean inner product). The function to maximize the time average is given componentwise by

$$\text{maximal} \stackrel{!}{=} \left\langle \sum_{i=1}^N q_i(t) \sum_{j=1}^N \mathbf{P}_{ij} q_j(t) \right\rangle_T = \sum_{i=1}^N \sum_{j=1}^N \langle q_i(t) q_j(t) \rangle_T \mathbf{P}_{ij} =: c. \quad (3.4)$$

Here, the so-called spatial correlation matrix $\mathcal{C}_{ij} = \langle q_i(t) q_j(t) \rangle_T$ arises, which is a discrete version of the spatial correlation function. (Here, this is literally true only for the periodic sinc basis. More accurately, it would be termed modal correlation matrix. In any case, it is not the temporal correlation matrix.) It is symmetric and positive semi-definite. After calculating an eigenbasis $\{\phi^i\}_{i=1, \dots, N}$ for \mathcal{C} we get

$$c = \sum_{i=1}^N \sum_{j=1}^N \sum_{k=1}^N \sum_{\alpha=1}^N \phi_k^i \mathbf{B}_{i\alpha} \lambda_k \mathbf{B}_{\alpha j}^\dagger \phi_k^j, \quad (3.5)$$

where ϕ_k^i denotes the k th component of the i th eigenvector of \mathcal{C} and λ_k is the k th eigenvalue. Since the columns of \mathbf{B} and the ϕ^i each form orthonormal sets and the λ_i 's are positive, (3.5) is maximized if we choose the eigenvectors ϕ^i for the largest eigenvalues of \mathcal{C} as columns of \mathbf{B} .

Now we have a method to obtain an optimal basis \mathbf{B} . To do this numerically, the correlation matrix is approximated by the sample correlation matrix \mathbf{C} . To determine \mathbf{C} the system is simulated using a finite number, e.g. N_t , of time steps which yields a data matrix $\mathbf{D}_{ij} = q_j(t_i)$. The sample correlation matrix is given by

$$\mathbf{C} = \frac{1}{N_t - 1} \mathbf{D}^\dagger \mathbf{D}, \quad (3.6)$$

where the number of time steps is N_t . Decomposing \mathbf{D} via the singular value decomposition (SVD), detailed in Golub & VanLoan (1983–1996), gives orthogonal matrices \mathbf{U} and \mathbf{V} and a diagonal matrix $\mathbf{\Sigma}$ with $\mathbf{D} = \mathbf{U}\mathbf{\Sigma}\mathbf{V}^\dagger$. The eigenbasis of \mathbf{C} is \mathbf{V} . This is obvious from $\mathbf{D}^\dagger \mathbf{D} = \mathbf{V}\mathbf{\Sigma}\mathbf{U}^\dagger \mathbf{U}\mathbf{\Sigma}\mathbf{V}^\dagger = \mathbf{V}\mathbf{\Sigma}^2 \mathbf{V}^\dagger$. In some cases the number of time steps N_t is much smaller than the spatial dimensionality N . In this case it is easier to calculate the eigenbasis \mathbf{U} of $\mathbf{D}\mathbf{D}^\dagger$. The matrix \mathbf{V} can then be obtained via $\mathbf{U}^\dagger \mathbf{D} = \mathbf{\Sigma}\mathbf{V}$. Since $\mathbf{\Sigma}$ is diagonal we only have to normalize the columns of $\mathbf{\Sigma}\mathbf{V}$ to get \mathbf{V} which is the eigenbasis of $\mathbf{D}^\dagger \mathbf{D}$ and consequently also of the correlation matrix $\mathbf{C} = (1/(N_t - 1))(\mathbf{D}^\dagger \mathbf{D})$. In the literature this is also known as method of snapshots.

4. Variational POD method

The POD method presented by Bogner (2007), here referred to as the POD-DMRG method, is based on density matrix renormalization group (DMRG) techniques. It is restricted to spatially one-dimensional systems by construction. For physical

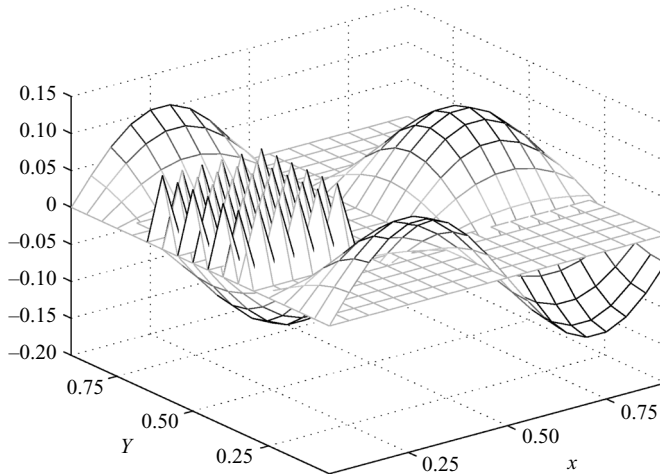


FIGURE 1. Illustration of one low-wavenumber Fourier mode and a set of delta states that make up one particular choice of B_{new} . The delta states are not shown normalized here.

applications this is a severe restriction. This problem is typical for DMRG applications and no complete solution to it has been found until now. However, some approaches to higher spatial dimensions exist for quantum mechanics. This work extends the POD-DMRG method to systems with higher spatial dimensionality in a way similar to the one presented by Martín-Delgado, Rodríguez-Laguna & Sierra (2001). The proposed method is described here. The quantum mechanical approach is not detailed further, since this is not necessary for the understanding. The same holds for the approach of Bogner (2007), which is technically quite independent from this work.

4.1. Technical implementation

The task is to find an optimal reduced basis of dimension M . The first step is to choose an ansatz basis \mathbf{B}^0 of dimension M . Principally, this could be a random but orthonormal basis. This is inefficient but works e.g. for the diffusion (or heat) equation $\partial q_C / \partial t = k \Delta q_C$. For the Navier–Stokes equations, instabilities arise in this case, since random basis functions are not likely to be smooth. A more sensible choice for the ansatz basis is e.g. a set of low-wavenumber Fourier modes. Here we always start with this initialization. The ansatz basis \mathbf{B}^0 is extended by a test basis \mathbf{B}_{new} containing a number of M_{patch} column vectors, which should be linearly independent of \mathbf{B}^0 . In the work of Martín-Delgado *et al.* (2001), delta states for a particular ‘patch’ region in the physical space are chosen but this is not mandatory. As an example, a set of delta states together with a Fourier mode is represented in figure 1 graphically. The resulting composed basis $\mathbf{B}^{0'} := [\mathbf{B}^0, \mathbf{B}_{new}]$ has size $N \times (M + M_{patch})$ and full rank. Via an orthonormalization procedure, e.g. Gram–Schmidt, we obtain the $N \times (M + M_{patch})$ orthonormal matrix $\mathbf{B}^{0''}$. The reduced system is now determined by $\mathbf{B}^{0''}$ via (2.8)–(2.10). The dynamics of the reduced system is given by (2.11), replacing \mathbf{B} with $\mathbf{B}^{0''}$. This system has $(M + M_{patch})$ degrees of freedom and is simulated in each iteration step. For the following iterations the construction of the corresponding matrices $\mathbf{B}^{i'}$, $\mathbf{B}^{i''}$ (for the i th iteration) is similar. As described in §3, we obtain an orthonormal POD basis $\tilde{\mathbf{B}}_{POD}$ of the reduced system, which we use to calculate the new improved ansatz basis (retaining M degrees of freedom)

$$\mathbb{R}^{N \times M} \ni \mathbf{B}^{i+1} = (\mathbf{B}^{i''})^\dagger \tilde{\mathbf{B}}_{POD}. \quad (4.1)$$

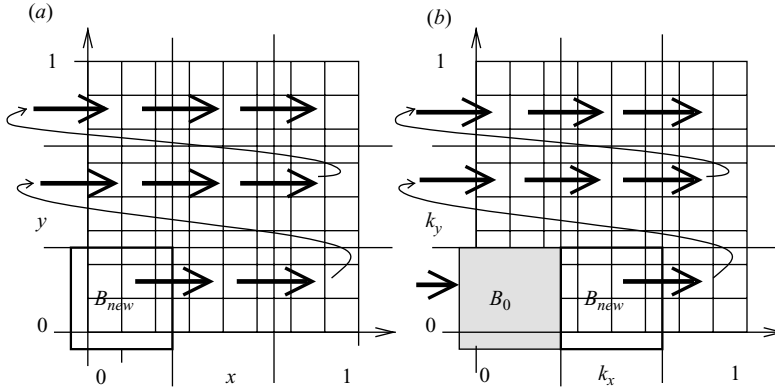


FIGURE 2. Scheme for choosing the inserted basis B_{new} . (a) For the real-space method choosing delta functions, one for each grid node in the current patch. (b) The same choice for the spectral variant in Fourier space. Since then B^0 is initialized with the lowest wavenumber vectors, starting with an adjacent patch is necessary.

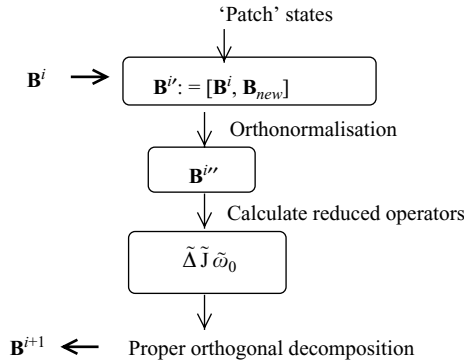


FIGURE 3. Flow chart diagram for a single step in the variational method. In each step the basis B^i is first expanded by B_{new} and, subsequently to the POD calculation, reduced to its original size again. An iteration step consists of several substeps, until all the inserted B_{new} together span the whole phase space. Here the reduced entities are the reduced Laplace operator $\tilde{\Delta}$, the reduced Jacobi operator \tilde{J} and the reduced initial condition $\tilde{\omega}_0$.

The basic step described above is now repeated with different choices for B_{new} . In the case of B_{new} being composed of delta states, one typically moves the ‘patch’ through the physical space. This is also done by Martín-Delgado *et al.* (2001) (see figure 2a). A single iteration step is completed when the full system has been covered by the patch, or more generally, when the matrices B_{new} of all iteration steps span the whole phase space. To improve the reduction, several iterations can be performed. In figure 3 we present a flow chart of the method proposed above.

4.2. Spectral variant

The choice of delta states for B_{new} in the method above results in a local inhomogeneous description of the field evolution. This can be problematic for the study of the incompressible Navier–Stokes equations as it enforces the occurrence of instabilities. A smoother approximation is obtained if one chooses B_{new} to be composed of low-wavenumber Fourier modes instead; then the ‘patching’ occurs in

Fourier space (see figure 2b). Since we require \mathbf{B}^i and \mathbf{B}_{new} to be linearly independent, one has to choose the first initialization accordingly.

4.3. Motivation of the term ‘variational method’

The term ‘variational method’ can be motivated as follows. We are searching for an optimal reduced basis and consequently for an optimal reduced model. The form of this model is always prescribed by (2.4). The optimality condition (3.4) describes a minimization problem where the only free parameters are the matrix elements of \mathbf{B} . Requiring orthonormality, not all matrix elements of \mathbf{B} are independent, but even without further constraints the columns of \mathbf{B} maximizing (3.4) and (3.5) would be linearly independent. In each iteration step the number of free parameters is temporarily increased. This corresponds to a variation of the reduced system. For an optimal \mathbf{B} the error functional to be minimized should not change under the variation. This is best approximated by our choice of \mathbf{B}^{i+1} for the next iteration. Here two points remain: First, it is assumed that calculation of the POD and the model reduction commute. Second, a higher dimensional model (expanded basis) will in general lead to higher accuracy. Therefore the eigenvectors, not included in \mathbf{B}^{i+1} , will correspond to non-zero eigenvalues in the correlation matrix. Consequently, the error functional will change under the variation. Nevertheless, for our choice of \mathbf{B}^{i+1} this change is minimal, under the constraint of having an M -dimensional reduced model.

5. Navier–Stokes equations and two-dimensional flows

The Navier–Stokes equations constitute a general framework for the description of the macroscopic variables of a fluid and thus have great practical importance. It should be noted that two-dimensional flow dynamics differs significantly from its three-dimensional counterpart. In two-dimensional flows, e.g. the effect of vortex stretching is absent. In three dimensions, if a vortex is stretched, the rotating fluid is moved to the vortex line. Conservation of angular momentum leads to an increase of angular velocity and the vortex can break up. In two dimensions the vorticity is always perpendicular to the plane of motion so that it can be described by a quasi-scalar. Due to this property energy is transported from smaller scales to larger scales. Hasegawa (1985) and van Heijst (1993) have considered this as an example for self-organization. Of fundamental importance for the self-organization is the process of merging of two equal-signed vortices. This has been studied e.g. by Nielsen *et al.* (1996). Two-dimensional flows can be observed, e.g. in stratified fluids. One important example is the atmosphere (e.g. see Dritschel & Legras 1993). There are also additional forces due to the rotating frame of reference as the Coriolis force have to be considered (see Huber, McWilliams & Ghil 2001). Variational methods have already been applied to the two-dimensional Euler flow for steady-state problems, e.g. by van de Fliert, van Grossen & de Vries (1995). The unforced incompressible viscous two-dimensional Navier–Stokes equation will be used as a testing ground for the method.

The equations for incompressible flow read

$$\rho \frac{\partial \mathbf{v}}{\partial t} = \mu \nabla^2 \mathbf{v} - \rho (\mathbf{v} \nabla) \mathbf{v} - \nabla p, \quad (5.1)$$

$$\nabla \cdot \mathbf{v} = 0. \quad (5.2)$$

Here ρ is the density, \mathbf{v} the velocity and μ the dynamic fluid viscosity. The Navier–Stokes equations can be rescaled to compare flows on different lengths L_0 and velocity

scales v_0 . Here the Reynolds number $Re := (v_0 L_0 \rho) / \mu$ characterizes the problem and describes the ratio of inertial forces to viscous forces. Therefore, the Reynolds number will be a relevant parameter in the present study. Here the rescaled dimensionless variables are always considered. In incompressible inviscid flows the vorticity $\int_{\Omega} \boldsymbol{\omega} dx$ and the kinetic energy $\mathcal{E} = (1/2) \int_{\Omega} \|\mathbf{v}\|^2 dx$ are conserved. In two-dimensional flows also the enstrophy $\mathcal{V} = (1/2) \int_{\Omega} \boldsymbol{\omega}^2 dx$ is conserved. For more details, see Kraichnan & Montgomery (1980).

For incompressible flows the flow velocity is completely determined by the vorticity $\boldsymbol{\omega}$ as

$$\mathbf{v} = \nabla \times \boldsymbol{\omega}. \quad (5.3)$$

Taking the curl of (5.1) and noting that the vorticity $\boldsymbol{\omega}$ is orthogonal to the plane onto which \mathbf{v} is restricted one gets the vorticity-stream function formulation:

$$\frac{\partial \omega}{\partial t} = \frac{1}{Re} \nabla^2 \omega - \frac{\partial \omega}{\partial x} \frac{\partial \psi}{\partial y} + \frac{\partial \omega}{\partial y} \frac{\partial \psi}{\partial x}, \quad (5.4)$$

where ω is the pseudo-scalar vorticity, i.e. the modulus of the vorticity $\boldsymbol{\omega}$, and ψ the stream function. The vorticity and the stream function are related via the Poisson equation

$$\nabla^2 \psi = -\omega. \quad (5.5)$$

Periodic boundary conditions in both spatial dimensions are used here. The spatial discretization is done by a spectral method which is detailed e.g. in Gottlieb & Orszag (1977). Here a finite set of low-wavenumber Fourier modes serves as ansatz functions for the discretized solution. The time integration is performed by a third-order stiffly stable operator splitting method which was proposed by Karniadakis, Israeli & Orszag (1990).

5.1. Model problem

To compare the reduction methods, the process of the merging of two adjacent vortices is used as an example. For the non-viscous case this process has been studied, e.g. by Nielsen *et al.* (1996). The initial conditions used in the following are a superposition of two equal-signed vortices, each given by

$$\omega_{\pm}(x, y) = \frac{1}{2} \zeta_0 \left(1 - \tanh \sqrt{\left(x - \frac{1}{2}\right)^2 + \left(y \pm d_h - \frac{1}{2}\right)^2} \right), \quad x, y \in [0, 1], \quad (5.6)$$

where ζ_0 denotes the initial maximal vortex intensity and $2d_h$ stands for the initial distance of the two vortices. These parameters are set to $\zeta_0 = 1$ and $d_h = 0.15$, respectively. Thus the initial condition is $\omega_0 := \omega(t_0, x, y) = \omega_+(x, y) + \omega_-(x, y)$. The computational domain is the square given by

$$\Omega = [0, 1] \times [0, 1]. \quad (5.7)$$

The time interval is

$$[t_0, t_{max}] = [0, 100]. \quad (5.8)$$

In the case of the incompressible flow the ordinary differential equation system resulting from the spatial discretization of (5.4) and (5.5) can be written as

$$\frac{d}{dt} \omega_i = \Delta_{i,j} \omega_j + J_{i,j,k} \omega_j \psi_k, \quad (5.9)$$

$$-\Delta_{i,j} \psi_j = \omega_i. \quad (5.10)$$

Use of Einstein's sum convention is made here. The equations for the reduced dynamics have the same form but contain the reduced operators and initial conditions

$$\tilde{\Delta}_{i,j} := B_{\alpha i} \Delta_{\alpha\beta} B_{\beta j}, \quad (5.11)$$

$$\tilde{J}_{i,j,k} := B_{\alpha i} J_{\alpha\beta\gamma} B_{\beta j} B_{\gamma k}, \quad (5.12)$$

$$\tilde{\omega}_{0i} := B_{\alpha i} \omega_{0\alpha}. \quad (5.13)$$

5.2. Numerical integration

Finite resolution tends to lead to instability of the numerical solution schemes for the Navier–Stokes equations. Nielsen *et al.* (1996) have mitigated this effect by an artificial hyper-viscosity term. In their work a spectral discretization and a third-order operator splitting scheme as proposed by Karniadakis *et al.* (1990) is used. The accuracy of all reduction methods has shown to decrease significantly for larger Reynolds numbers. Therefore these studies are restricted to comparatively low Reynolds numbers of $Re \leq 800$.

6. Numerical results

The flow described above is analysed for grid sizes of 48×48 and 72×72 using spectral methods for spatial discretization and a third-order time integration. The resolution is considerably low for studies of such types of problems. The aim is to test the approach on a minimalist model. Nevertheless, the small system size provides fast calculations and also mitigates the need to optimize the efficiency of the algorithms considered here. It reduces possible error sources also.

Throughout this section the L^2 -error of the reduced and full simulation is considered. It is defined by

$$E_{L^2}(t) := \int_{\Omega} (q(x, t) - \tilde{q}(x, t))^2 dx, \quad (6.1)$$

where $\tilde{q}(x, t)$ is the reduced field and results from the expansion in (2.2), replacing \mathbf{q} by \mathbf{Pq} . The L^2 -error, E_{L^2} , is identical to the error already introduced in (2.13) multiplied by $1/\sqrt{N}$ due to the orthonormality of the expansion functions (see (2.3)) and since

$$\int_{\Omega} dx = 1, \quad \left(\sum_{i=1}^N 1 \right)^{1/2} = \sqrt{N}. \quad (6.2)$$

Note that the spectral variant of the variational POD algorithm is used, unless otherwise stated explicitly.

6.1. Snapshots of the flow

To give a qualitative idea of the merging process, a series of snapshots of the vorticity field for Reynolds number $Re = 400$ are included. For lower values of Re the influence of friction increases, leading to a faster decrease of the vorticity and a 'less interesting' dynamics. Figure 4 shows the time evolution of the vorticity in three-dimensional plots. During the simulation both vortices merge after encircling each other for about $2/3$ rotations leaving a large vortex with some additional structure.

6.2. Comparing the accuracy

6.2.1. Effect of the Reynolds number

To compare the quality of the different reduction methods, the L^2 -error for the standard POD, the variational POD and a low-wavenumber Fourier mode reduction

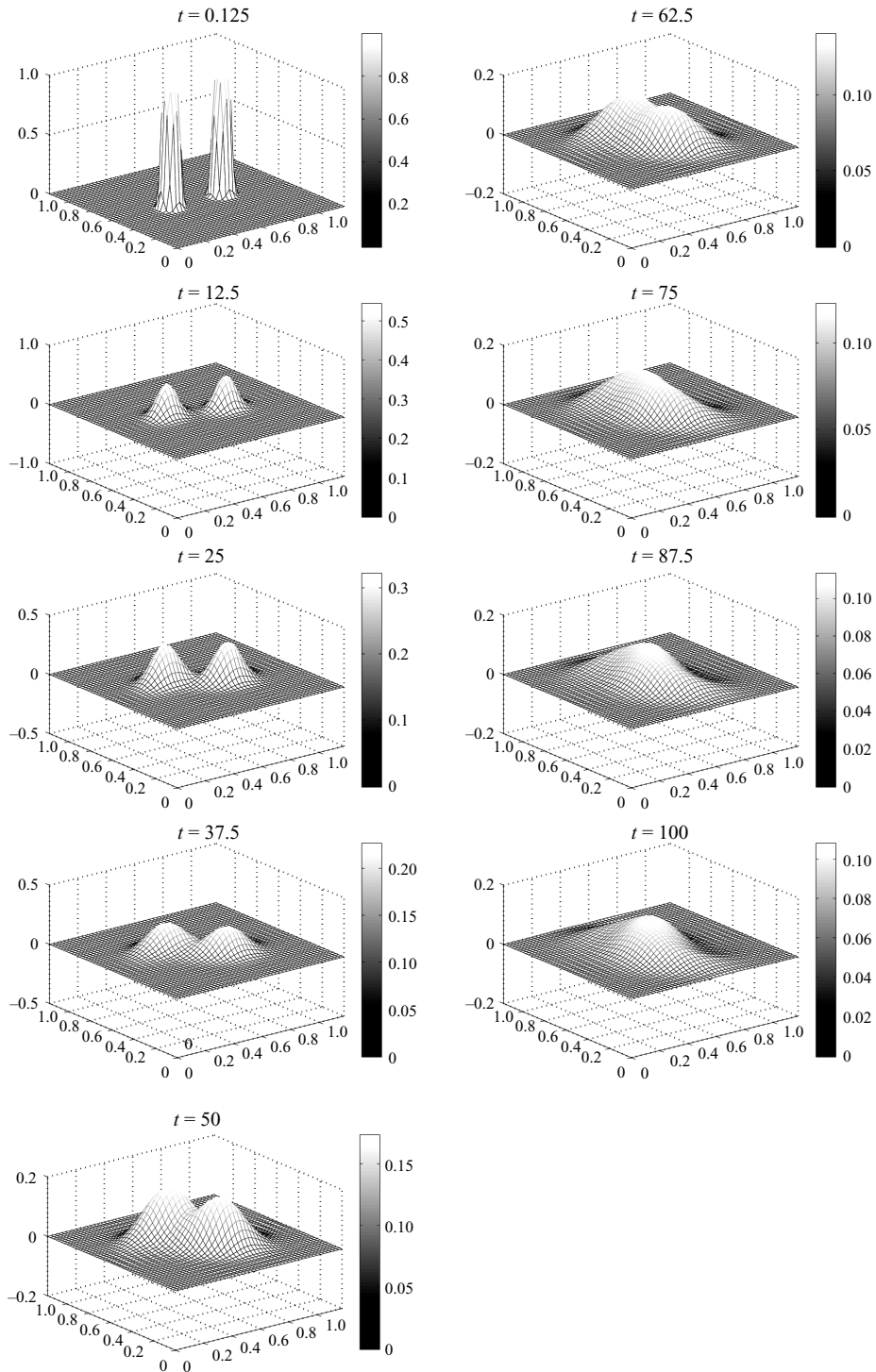


FIGURE 4. Vorticity for the 48×48 grid at $Re = 400$ after 1–800 time steps as three-dimensional plots. At $t = 100$ approximately $2/3$ rotations of the vortices around each other are completed.

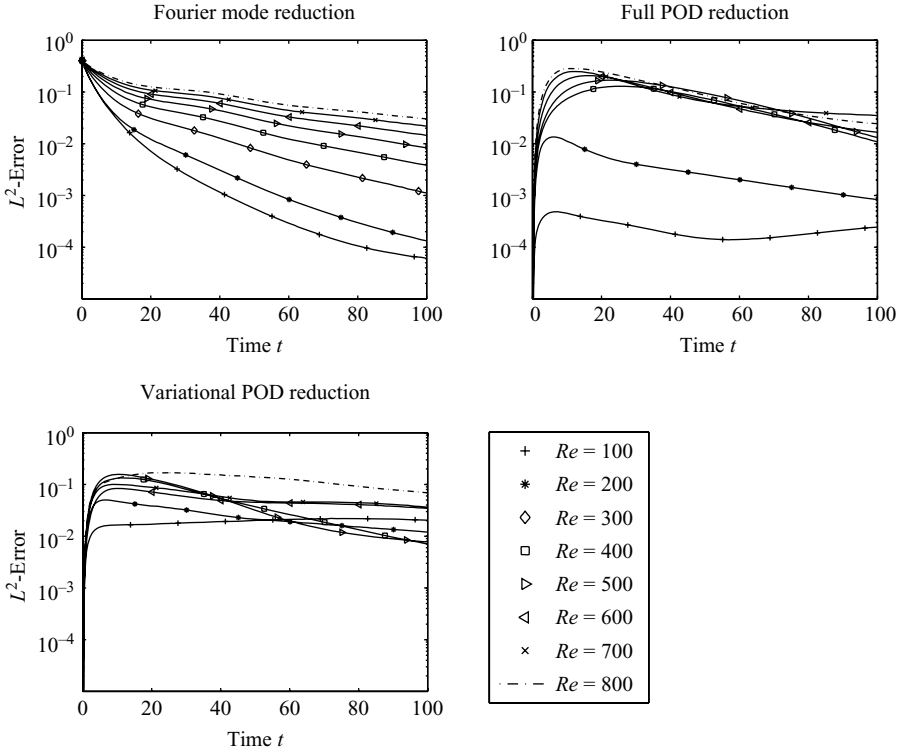


FIGURE 5. L^2 -error for $Re = 100$ to $Re = 800$, three iteration runs, $h_t = 0.125$, $M = 36$, $M_{patch} = 36$ and 800 time steps.

is calculated. Figure 5 shows the results for a 48×48 grid, a time step of $h_t = 0.125$ and a Reynolds number range from 100 to 800. For the variational algorithm the number of retained states M as well as the number of trial states M_{patch} is $M = 36$, $M_{patch} = 36$. The simulation time is long enough so that a final state with a single broad vortex is reached (compare also figure 4).

A decrease in performance is observed for increasing Reynolds number for all methods. For low Reynolds number the Fourier mode reduction is superior to the other methods. The good performance of the low-wavenumber Fourier mode reduction results from the special properties of the problem at hand. In this special case the diffusion as well as the two-dimensional advection mainly produce structures on large length scales. This result does not reduce the value of the variational POD approach as both POD-based methods compared here do not rely on a particular dynamical system.

The full POD reduction gives very similar performance for Reynolds numbers $Re \geq 400$. The errors produced by the variational POD reduction are comparable to the ones obtained by the full POD reduction. For the higher Re numbers the upper error bound is lower for the variational POD reduction, compared to the standard POD as well as to the Fourier reduction.

6.2.2. Effects of the iterations

The aim of the iterations, or sweeps, is to increase the accuracy of the reduced model. The corresponding error calculations are shown in figure 6. It can be stated that the desired result is obtained only for the Reynolds number $Re = 400$ which lies

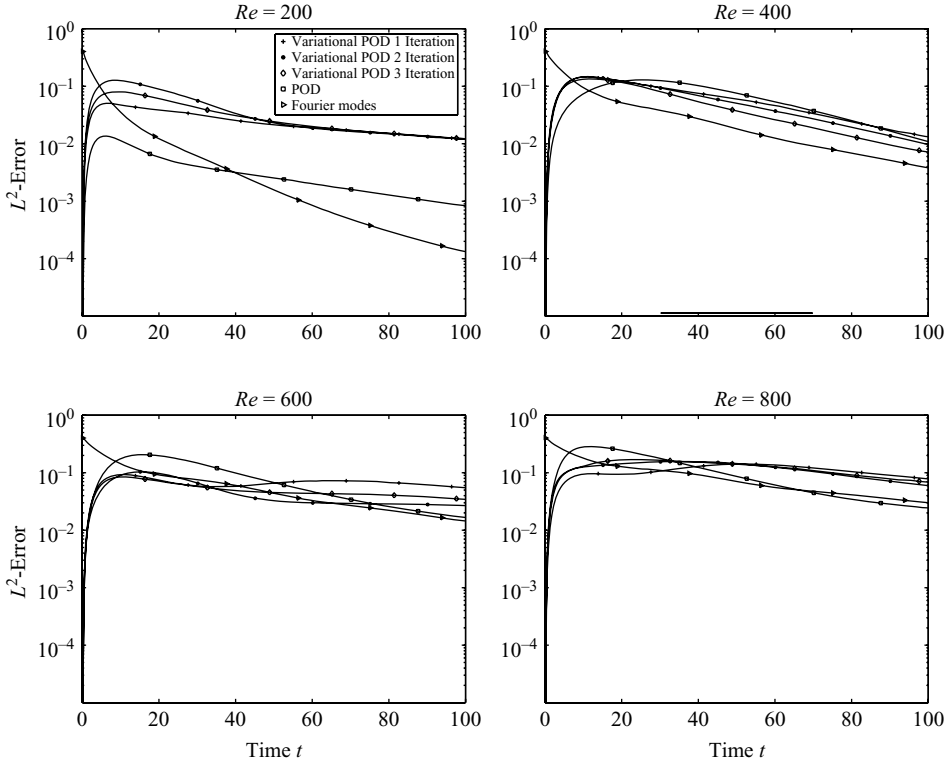


FIGURE 6. The L^2 -error for the 48×48 -dimensional grid with Reynolds numbers from $Re = 200$ to 800 . The time step size is $h_t = 0.125$ and the numbers of retained and trial states are $M = M_{patch} = 36$.

also in the domain, where the variational POD performs best. In the other cases the iterations may even decrease the accuracy. It can be concluded that a single iteration is in these cases enough and further steps do not gain more information. This is clearly undesirable; however, the source of this behaviour is yet unknown.

6.2.3. Effects of different number of retained states

The number of retained states M determines the dimensionality of the reduced system and therefore affects the accuracy of the reduced model directly. The number of trial states M_{patch} is chosen equal to M . To compare the performance of the different modes, the system is simulated using M modes. The L^2 -error with respect to the full simulation is calculated. The result for the Reynolds number $Re = 150$ is shown in figure 7. Only a marginal reduction of the error is observed for increasing M for the standard POD method. This would be expected if already a few POD modes are sufficient to describe the dynamics efficiently. However, the performance of the low-wavenumber Fourier mode basis is for significant time spans superior to that of the standard POD modes. For the Fourier mode reduction itself one observes a very systematic increase of the accuracy with M . Therefore one can conclude that the Fourier modes of the lowest 12×12 wavenumbers are all relevant for the dynamics. Especially the initial conditions are very localized and so many Fourier modes are necessary for a good approximation. The variational POD modes show a tendency to a poorer performance than the standard POD results. This occurs approximately in the

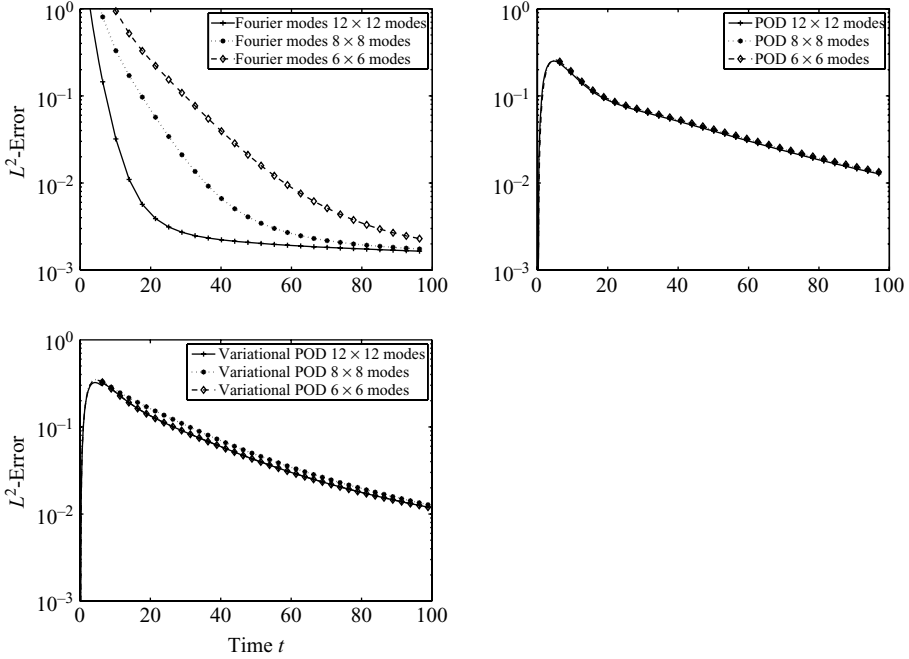


FIGURE 7. L^2 -error for $Re = 150$, comparing $M = 36$, $M_{patch} = 36$, $M = 64$, $M_{patch} = 64$ and $M = 144$, $M_{patch} = 144$ for the numbers of retained and trial states. Three iteration runs with the spectral variant of the variational POD method are used, $h_t = 0.125$ and 3200 time steps.

time domain in which the standard POD results are also superior to the Fourier mode reduction. Further a small decrease of accuracy is observed when increasing M from 36 to 64. This is surprising and currently no complete explanation is available. The choice of M and M_{patch} directly affects the calculation of the modes for the variational POD method in contrast to the low-wavenumber Fourier or standard POD modes. Additional modes in the variational POD method can then in principle contribute to numerical artefacts instead of increasing the quality of the approximation. However, the expected increase of accuracy is observed when increasing M further to 144.

6.2.4. Effect of the spatial resolution

The resolution of the lattice clearly determines the accuracy of the unreduced system in describing the partial differential equation of interest. To assess the impact of this parameter on the quality of the reduction, calculations on the usual 48×48 grid and on a 72×72 grid are performed. Both lattice sizes are integer multiples of 6×6 and in both cases $M = 36$, $M_{patch} = 36$ are chosen. By this choice the reduced systems have the same dimensionality in all cases. The other parameters are set exemplarily to $Re = 400$ and $h_t = 0.125$. A single iteration run is performed. The results are shown in figure 8. The effect of increasing the lattice resolution on the Fourier mode reduction and the POD mode reduction is comparatively small, below 10%. In case of the Fourier mode reduction this is on the one hand because the essentially same low-wavenumber Fourier modes (albeit with a higher resolution) are used. On the other hand the higher resolution does not lead to a qualitative different behaviour of the unreduced system. Thus one can assume that the resolution is high enough to give a good approximation to the continuous description. This assumption

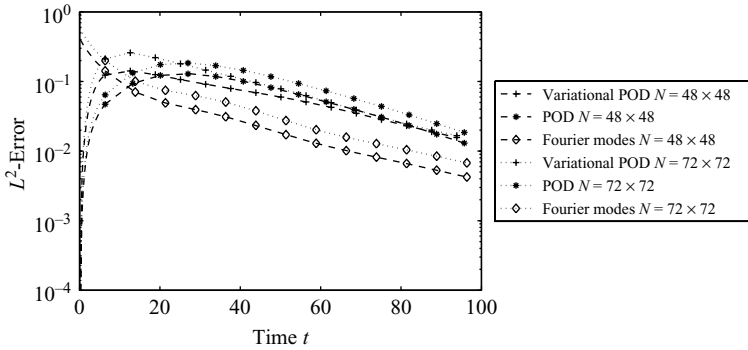


FIGURE 8. Comparison of the L^2 -error for a 48×48 and a 72×72 spatial grid. The numbers of retained and trial states are $M = 36$, $M_{patch} = 36$, the Reynolds number $Re = 400$ and the number of time steps $h_t = 0.125$. A single iteration run with 800 time steps is performed.

is supported by the small increase of accuracy for the POD reduction. The results for the variational POD method are also similar. The maximal error is higher for the increased resolution for all reduction methods. In contrast to the other approaches, the difference in the error due to the resolution decreases with time for the variational POD. This can be only contributed to the fact that there are more simulation steps in each iteration and that the test basis \mathbf{B}_{new} have a higher resolution also.

6.2.5. Variational POD versus the spectral variant

Comparing the performance of both versions of the variational POD one observes that the real-space variant is superior for $Re = 400$ but leads to higher errors than the other method for higher Reynolds numbers. For $Re = 500$ the maximum error is still smaller than for the other approaches. The reason for this behaviour is not yet clear. For $Re = 200$ the real-space algorithm did not even converge, i.e. the simulation of the reduced system breaks down. Thus the spectral version of the variational POD reduction seems to be preferable to the real-space variant. The spectral variant is also successful in a broader Reynolds number domain (see figure 9).

6.2.6. Visualization of the POD and V-POD modes

The POD modes themselves can visualize some qualitative aspects of the flow. Therefore the most relevant modes for the full POD and the variational POD are shown in figures 10 and 11. For the first example with $Re = 200$ one sees a qualitative agreement with the POD method although the variational POD modes seem to be degraded. The second example shows the results of the real-space method for $Re = 400$ which are clearly superior to those of the standard POD. Subjectively these modes seem to be more inaccurate than the POD modes. From this one can state that the quality of the reduced basis is not intuitively accessible from the modes themselves.

6.2.7. Stability

For numerical calculations stability is an important concern. Two points are of relevance here. First, it has to be ensured that the time averages (see (3.1)), can be calculated numerically. The dynamical system is considered in a discretized form. Therefore a suitable choice of the spatial and temporal discretization, which is not a subject of this work, is required. An inadequate choice of the discretization can cause instabilities that are not connected to the proposed method. However, this topic should be kept in mind when choosing \mathbf{B}_0 or \mathbf{B}_{new} . In practice, only predictably

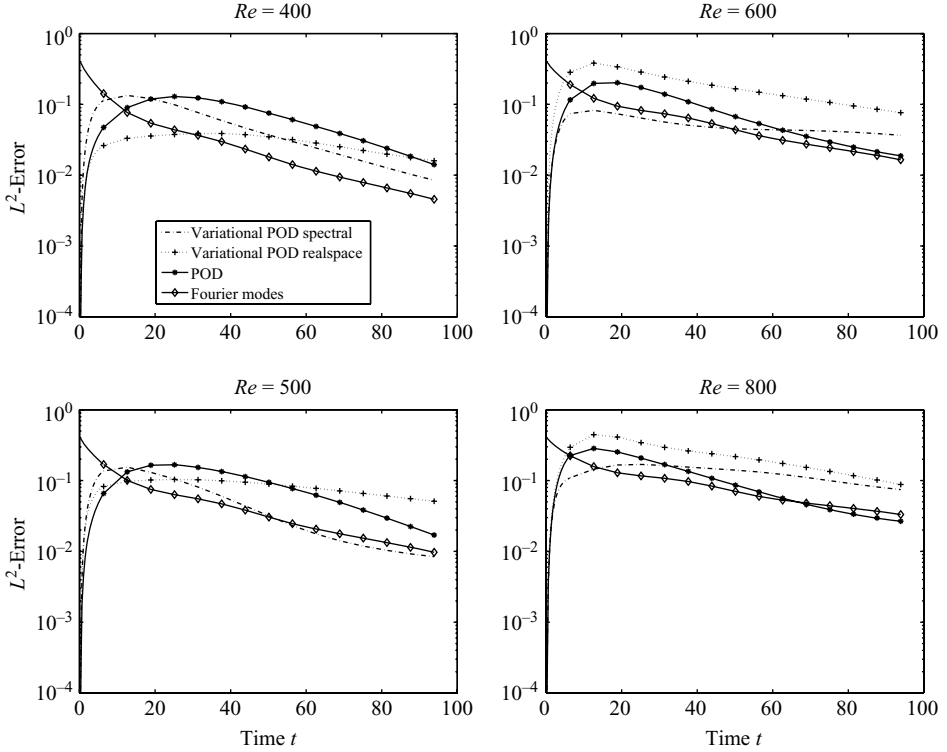


FIGURE 9. Comparison of the real-space method with the spectral variant of the variational POD method. The L^2 -error for the 48×48 -dimensional grid with Reynolds numbers, Re from 400 to 800. The time step size is $h_t = 0.125$ and the number of retained and trial states $M = M_{patch} = 36$.

inappropriate choices, as a random basis or delta states in real-space for larger Reynolds numbers, have caused problems. In order to have a stable system, the eigenvalues of the generator of the time evolution have to be zero or negative. The proposed method basically replaces the simulation in the standard POD approach by repeated simulation runs of small subsystems. Therefore the time averages for the subsystems have to be calculated. For a linear system the eigenvectors of the sample correlation matrix typically are also eigenvectors of the generator of the time evolution. The reduced generator of evolution, $\tilde{G} = \tilde{L}$, will then contain the largest eigenvalues of L which are less than or equal to 0 for stable systems. Then the reduced system is also stable and the time averages can be calculated. In the nonlinear case the reduced system may become unstable. Consequently, no sample correlation matrix can be calculated and the algorithm breaks down. In order to prevent this, the above points should be considered.

The second point is the stability of the algorithm itself, i.e. whether an improved reduction can be calculated if the time averages exist. For linear systems the iterations of the algorithm increase the quality of the reduction, once the calculation of the sample correlation matrix is guaranteed, by construction. Consider B_i and B_{new} to be L -invariant. The optimal L retains the M largest eigenvalues of L (see Bogner 2007). By construction, $B_{i+1}^\dagger L B_{i+1}$ will contain the M largest eigenvalues of $B_i^\dagger L B_i$ and $B_{new}^\dagger L B_{new}$. Therefore it will describe a more optimal reduced system. For nonlinear

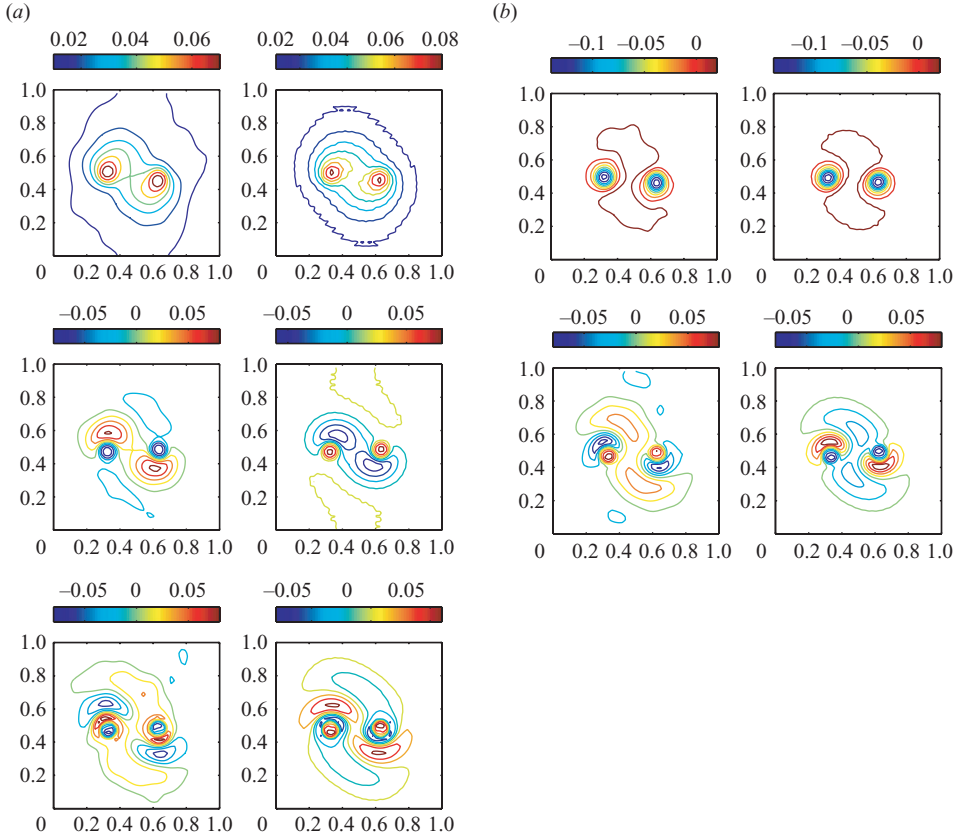


FIGURE 10. First five POD-modes for $Re = 200$, $M = 64$, $M_{patch} = 64$, three iteration runs using the spectral variant of the variational POD method with $h_t = 0.125$ and 3200 time steps. (a) Variational POD modes versus (b) full POD modes.

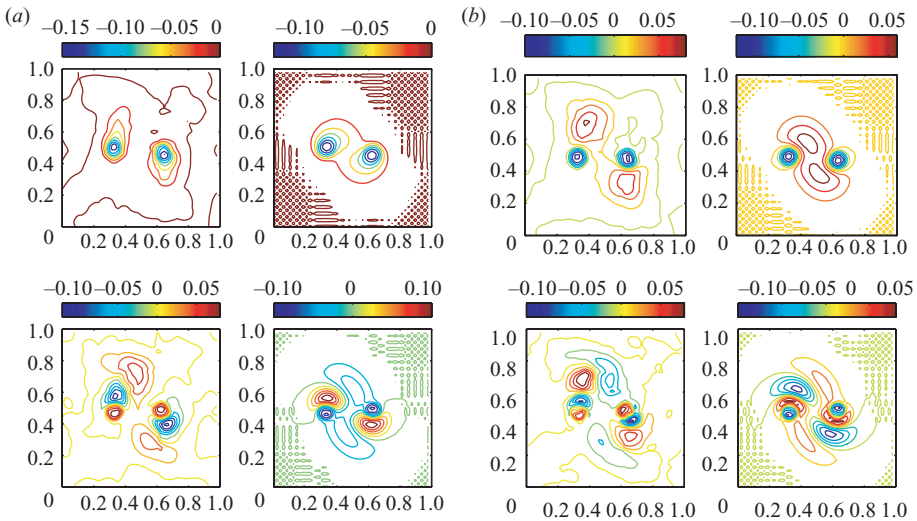


FIGURE 11. First four POD modes for $Re = 400$, $M = 36$, $M_{patch} = 36$, three iteration runs using the real-space variant of the variational POD method with $h_t = 0.125$ and 800 time steps. (a) Variational POD modes versus (b) full POD modes.

problems there is currently no rigorous proof, when an iteration step decreases the error. However, the diagonalization of the sample correlation matrix is well defined in any case. The algorithm further leads to an improvement in most cases considered here. If the accuracy is not increased, the additional error is small and can be removed in further steps.

7. Conclusions

Encouraged by the results of the POD-DMRG algorithm, this approach was extended to higher dimensional systems. As a model system the two-dimensional Navier–Stokes equations have been chosen. These are numerically more demanding than the examples considered by Bogner (2007) and describe a more realistic system. The algorithm itself can be interpreted as a variational form of the POD. One important point is that it can also be applied to higher dimensional systems without significant modifications. To restrict the numerical effort, the situation for a particular minimalist problem was evaluated only. This nevertheless demonstrates the viability of the approach and the simplicity encourages the use in non-fluid dynamical applications.

Although no previous simulation of the system is required, the performance of the variational POD was found to be comparable to the standard POD. The simulation is effectively split into several much simpler calculations. This is the main motivation for this approach. Currently, the simulation of the small reduced system poses the largest problems. The real-space variant, for example, has shown an unexplained divergence for low Reynolds numbers $Re \leq 200$. Nevertheless, the real space as well as the spectral variant of the variational POD exhibit a performance clearly superior to the full POD reduction and the Fourier mode reduction for a narrow Reynolds number range. This is possible since the POD reduction is optimal only for representing the simulation data. The reproduction of the dynamics itself need not to be optimal.

In particular for applications to fluid dynamics, care should be taken to start from a reasonable, i.e. stable, reduced system. The key is to find appropriate ansatz functions. These are subsequently improved by the variational POD. For more realistic problems more detailed understanding of flow processes should be included, e.g. a base flow could be included. If the equations are in velocity/pressure formulation, additional corrections to the pressure term, as in Noack, Papas & Monkewitz (2005), should be considered. Also effects of unresolved scales could lead to (stabilizing) higher order interactions as in Ukeiley *et al.* (2001). Compared with the Fourier mode reduction, the performances of all POD-based methods were inferior for the minimalist example in this work. This is problem dependent. Both the diffusion and the two-dimensional advection mainly lead to spatially low-frequency modes. Comparison of both POD-based approaches however shows that the variational POD can produce results similar to those produced by the standard POD. In contrast to the Fourier mode reduction, the POD methods rely less extensively on special properties of the system at hand.

No comparison of the computational load for the variational POD method and that for the standard POD was made. The reason for this is simple. The new approach requires the explicit storing and processing of dense (but comparatively small) matrices and tensors. Calculating a full POD with the same algorithms (e.g. for simulating the system) would be very inefficient and would result in an unrealistic high load for the full POD. If efficiency is an issue, the full POD and the variational POD have very different requirements. Therefore, comparison of the computational

load would depend too much on the choice of the actual implementation rather than on the methods themselves. Since the proposed method aims at avoiding the full simulation for a POD and thus eventually in a reduction of the computational load, at least a scaling argument for this approach should be given. The number of multiplications required by the variational POD increases linearly with the system size N . For the full simulation the computational load of a single time step scales at least with $N \log N$, depending on the time integration scheme. Further, the cost for the eigen decomposition of the sample covariance matrix is $(\min(N_t, N))^3$ for the standard POD, in contrast to $(\min(N_t, M + M_{patch}))^3$ for the variational POD. This would make the latter approach preferable for large N_t .

I would like to thank the German Science Foundation (DFG) for support of this project (Contract No. DE 896/1-(1,2) 2004-2007). Further I would like to thank Ph. Blanchard, F. Schmid, Birgit Lessmann and Hans Behringer for discussions.

REFERENCES

- ANTOULAS, A. C. 2005 *Approximation of Large-Scale Dynamical Systems*. Cambridge University Press.
- BERKOOZ, G., HOLMES, P. & LUMLEY, J. L. 1998 *Turbulence, Coherent Structures, Dynamical Systems and Symmetry*. Cambridge Monographs on Mechanics.
- BOGNER, T. 2007 Density matrix renormalization for model reduction in nonlinear dynamics. ArXiv Physics e-prints ArXiv:0707.4384v1.
- BUI-THANH, T., DAMODARAN, M. & WILLCOX, K. 2003 Proper orthogonal decomposition extensions for parametric applications in transonic aerodynamics. *AIAA Paper 4213*.
- DRITSCHEL, D. G. & LEGRAS, B. 1993 Modeling oceanic and atmospheric vortices. *Phys. Today* **46**, 44–51.
- VAN DE FLIERT, B. W., VAN GROESEN, E., R. DE ROO & DE VRIES, R. W. 1995 Numerical algorithm for the calculation of nonsymmetric dipolar and rotating monopolar vortex structures. *J. Comput. Appl. Math.* **62**, 1–25.
- GENTRY, R., MARTIN, R. & DALY, B. 1966 An Eulerian differencing method for unsteady compressible flow problems. *J. Comput. Phys.* **1**, 87–118.
- GOLUB, G. H. & VANLOAN, C. F. 3rd Edition 1996 *Matrix Computations*. Johns Hopkins University Press.
- GOTTLIEB, D. & ORSZAG, S. A. 1977 *Numerical Analysis of Spectral Methods: Theory and Application*. SIAM.
- HASEGAWA, A. 1985 Self-organization processes in continuous media. *Adv. Phys.* **34**, 1–42.
- VAN HEIJST, G. 1993 Self-organization of two-dimensional flows. *Nederlands Tijdschrift voor Natuurkunde* **59**, 321–325.
- HUBER, M., McWILLIAMS, J. C. & GHIL, M. 2001 A climatology for turbulent dispersion in the troposphere. *J. Atmos. Sci.* **58**, 2377–2394.
- KARNIADAKIS, G. E., ISRAELI, M. & ORSZAG, S. 1990 High-order splitting methods for the incompressible Navier–Stokes equation. *J. Comput. Phys.* **97**, 414–443.
- KRAICHNAN, R. H. & MONTGOMERY, D. 1980 Two-dimensional turbulence. *Reports Prog. Phys.* **43**, 547–619.
- LANDAU, L. D., LIFSCHITZ, E. M. & WELLER, W. 1991 *Hydrodynamik*, 5th rev. edn. Akademie-Verlag.
- LEIPHOLZ, H. 1974 *Theory of Elasticity*. Leyden, Noordhoff.
- LORENZ, E. N. 1956 Empirical orthogonal functions and statistical weather prediction. *Scientific Report 1*, Statistical Forecasting Project MIT.
- LUMLEY, J. L. 1967 *The Structure of Inhomogeneous Turbulent Flows*. Nauka.
- MARTÍN-DELGADO, M. A., RODRÍGUEZ-LAGUNA, J. & SIERRA, G. 2001 Single-block renormalization group: quantum mechanical problems. *Nucl. Phys. B* **601**, 569–590.
- NIELSEN, A. H., HE, X., RASMUSSEN, J. J. & BOHR, T. 1996 Vortex merging and spectral cascade in two-dimensional flows. *Phys. Fluids* **8**(9), 2263–2265.

- NOACK, B. R., AFANASIEV, K., MORZYNSKI, M., TADMOR, G. & THIELE, F. 2003 A hierarchy of low dimensional models for the transient and post-transient cylinder wake. *J. Fluid Mech.* **497**, 335–363.
- NOACK, B., PAPAS, P. & MONKEWITZ, P. 2005 The need for a pressure-term representation in empirical Galerkin models of incompressible shear flows. *J. Fluid Mech.* **523**, 339–365.
- ROWLEY, C. W., COLONIUS, T. & MURRAY, R. M. 2003 Model reduction of compressible flows using POD and Galerkin projection. *Phys. D* **189**, 115–129.
- SIROVICH, L. 1987 Turbulence and the dynamics of coherent structures. *Q. Appl. Math.* **XLV**, 561–591.
- UKEILEY, L., CORDIER, L., MANCEAU, R., DELVILLE, J., GLAUSER, M. & BONNET, J. 2001 Examination of large-scale structures in a turbulent plane mixing layer. Part 2. Dynamic systems model. *J. Fluid Mech.* **441**, 67–108.